

# A coordinate-independent characterization of a black hole shadow

A. A. Abdujabbarov,<sup>1,2,3</sup> L. Rezzolla<sup>4,5</sup> and B. J. Ahmedov<sup>1,2,3</sup>

<sup>1</sup>*Institute of Nuclear Physics, Ulughbek, Tashkent 100214, Uzbekistan*

<sup>2</sup>*Ulugh Beg Astronomical Institute, Astronomicheskaya 33, Tashkent 100052, Uzbekistan*

<sup>3</sup>*National University of Uzbekistan, Tashkent 100174, Uzbekistan*

<sup>4</sup>*Institut für Theoretische Physik, Max-von-Laue-Str. 1, D-60438 Frankfurt, Germany*

<sup>5</sup>*Frankfurt Institute for Advanced Studies, Ruth-Moufang-Str. 1, D-60438 Frankfurt, Germany*

13 September 2018

## ABSTRACT

A large international effort is under way to assess the presence of a shadow in the radio emission from the compact source at the centre of our Galaxy, Sagittarius A\* (Sgr A\*). If detected, this shadow would provide the first direct evidence of the existence of black holes and that Sgr A\* is a supermassive black hole. In addition, the shape of the shadow could be used to learn about extreme gravity near the event horizon and to determine which theory of gravity better describes the observations. The mathematical description of the shadow has so far used a number of simplifying assumptions that are unlikely to be met by the real observational data. We here provide a general formalism to describe the shadow as an arbitrary polar curve expressed in terms of a Legendre expansion. Our formalism does not presume any knowledge of the properties of the shadow, e.g., the location of its centre, and offers a number of routes to characterize the distortions of the curve with respect to reference circles. These distortions can be implemented in a coordinate independent manner by different teams analysing the same data. We show that the new formalism provides an accurate and robust description of noisy observational data, with smaller error variances when compared to previous approaches for the measurement of the distortion.

**Key words:** black hole physics – Galaxy: centre – submillimetre: galaxies

## 1 INTRODUCTION

There is a widespread belief that the most convincing evidence for the existence of black holes will come from the direct observations of properties related to the horizon. These could be through the detection of gravitational waves from the collapse to a rotating star (Baiotti & Rezzolla 2006), from the ringdown in a binary black hole merger (Berti et al. 2009), or through the direct observation of its ‘shadow’. In a pioneering study, Bardeen (1973) calculated the shape of a dark area of a Kerr black hole, that is, its ‘shadow’ over a bright background appearing, for instance, in the image of a bright star behind the black hole. The shadow is a gravitationally lensed image of the event horizon and depends on the closed orbits of photons around the black hole<sup>1</sup>. Its outer boundary, which we will hereafter simply refer to as the shadow, corresponds to the apparent image of the photon capture sphere as seen by a distant observer. General relativity predicts, in fact, that photons circling the black hole slightly inside the boundary of the photon sphere

will fall down into the event horizon, while photons circling just outside will escape to infinity. The shadow appears therefore as a rather sharp boundary between bright and dark regions and arises from a deficit of those photons that are captured by the event horizon. Because of this, the diameter of the shadow does not depend on the photons’ energy, but uniquely on the angular momentum of the black hole. In general relativity and in an idealized setting in which everything is known about the emission properties of the plasma near the black hole, the shadow’s diameter ranges from  $4.5 r_s$  for an extreme Kerr black hole, to  $\sqrt{27} r_s$  for a Schwarzschild black hole, where  $r_s := 2GM/c^2$  is the Schwarzschild radius. In practice, however, the size and shape of the shadow will be influenced by the astrophysical properties of the matter near the horizon and, of course, by the theory of gravity governing the black hole.

Besides providing evidence on the existence of black holes, the observation of the black hole shadow and of the deformations resulting in the case of nonzero spin, is also expected to help determine many of the black hole properties (see e.g. Chandrasekhar 1998; Falcke & Markoff 2013; Takahashi 2004; Falcke et al. 2000; Doeleman et al. 2009). More specifically, imaging the shadow of a black hole via radio observations will allow one to test the predictions of general relativity for the radius of the shadow and study astrophysical phenomena in the vicinity of black holes [see Johannsen & Psaltis (2010) and, more recently, Zharov (2014) for

<sup>1</sup> Strictly speaking, also an horizon-less object such as a gravastar (Mazur & Mottola 2004) would lead to a shadow. However, rather exotic assumptions on the heat capacity of the gravastar’s surface are needed to justify a lack of emission from such a surface (Broderick & Narayan 2007); gravitational-wave emission would unambiguously signal the presence of an event horizon (Chirenti & Rezzolla 2007).

a review]. In addition, it will allow one to set constraints on the validity of alternative theories of gravity which also predict black holes and corresponding shadows (see e.g. [Eiroa & Sendra 2014](#); [Tsukamoto et al. 2014](#); [Falcke & Markoff 2013](#)).

The possible observation of a black hole shadow has recently received a renewed attention as the spatial resolution attainable by very long baseline interferometry (VLBI) radio observations is soon going to be below the typical angular size of the event horizon of candidate supermassive black holes (SMBHs), such as the one at the centre of the Galaxy or the one in the M87 galaxy ([Falcke et al. 2000](#)). These observations are the focus of international scientific collaborations, such as the Event Horizon Telescope (EHT)<sup>2</sup> or the Black Hole Camera (BHC)<sup>3</sup>, which aim at VLBI observations at 1.3 mm and 0.87 mm of Sagittarius A\* (Sgr A\*) and M87. We recall that Sgr A\* is a compact radio source at the centre of the Galaxy and the SMBH candidate in our galaxy. In fact, the orbital motion of stars near Sgr A\* indicates that its mass is  $\simeq 4.3 \times 10^6 M_\odot$  ([Ghez et al. 2008](#); [Genzel et al. 2010](#)).

Given a distance of 8 kpc from us, the angular size of the Schwarzschild radius of the SMBH candidate in Sgr A\* is  $\sim 10 \mu\text{as}$ , so that the corresponding angular diameter of the shadow is of the order of  $\sim 50 \mu\text{as}$ . Similarly, with an estimated mass of  $\simeq 6.4 \times 10^9 M_\odot$  ([Gebhardt et al. 2011](#)) and a distance of 16 Mpc, the M87 galaxy represents an equally interesting SMBH candidate, with an angular size that is of the same order i.e.,  $\sim 40 \mu\text{as}$ . Although the resolution achievable at present is not sufficient to observe an image of the shadow of either black hole, it is sufficiently close that it is realistic to expect that near-future observations will reach the required resolution. Indeed, future EHT and BHC observations of Sgr A\* are expected to go below the horizon scale and to start to provide precise information on the black hole orientation, as well as on the astrophysical properties of the accretion flow taking place on to the black hole ([Chan et al. 2015](#); [Psaltis et al. 2015](#)).

An extensive literature has been developed to calculate the shadow of the black hole in known space-times, either within general relativity ([Young 1976](#); [Perlick 2004](#); [Abdujabbarov et al. 2013](#)), or within alternative theories of gravity ([Bambi & Modesto 2013](#); [Tsukamoto et al. 2014](#); [Amarilla et al. 2010](#); [Amarilla & Eiroa 2012, 2013](#); [Atamurotov et al. 2013a,b](#); [Schee & Stuchlík 2009](#)). In most cases, the expression of the shadow as a closed polar curve is not known analytically, but for the Plebański-Demiański class of space-times, the shadow has been cast in an analytic form ([Grenzebach et al. 2014, 2015](#)).

Because the shadow is in general a complex polar curve on the celestial sky, an obvious problem that emerges is that of the characterization of its deformation. For example, in the case of a Kerr black hole, the difference in the photon capture radius between corotating and counter-rotating photons creates a “dent” on one side of the shadow, whose magnitude depends on the rotation rate of the black hole. A way to measure this deformation was first suggested by [Hioki & Maeda \(2009\)](#) and then further developed by other authors ([Bambi & Freese 2009](#); [Bambi & Yoshida 2010](#); [Bambi & Modesto 2013](#)). In essence, in these approaches the shape of the shadow is approximated as a circle with radius  $R_s$  and such that it crosses through three points located at the poles and at the equator of the shadow’s boundary. The measure of the dent is then made in terms of the so called ‘deflection’, that is, the difference between the endpoints of the circle and of the shadow, with a di-

dimensionless distortion parameter being given by the ratio of the size of the dent to the radius  $R_s$  [cf. Eq. (48)].

While this approach is reasonable and works well for a black hole such as the Kerr black hole, it is not obvious it will work equally well for black holes in more complex theories of gravity or even in arbitrary metric theories of gravity as those considered by [Rezzolla & Zhidenko \(2014\)](#). Leaving aside the fact in all these works the shadow is assumed to be determined with infinite precision (an assumption which is obviously incompatible with a measured quantity), many but not all approaches in characterizing the black hole shadow and its deformations suffer from at least three potential difficulties. They often assume a primary shape, i.e., that the shadow can be approximated with a circle; exceptions are the works of [Kamruddin & Dexter \(2013\)](#) and [Psaltis et al. \(2014\)](#). In the first one, a model has been proposed to describe the “crescent” morphology resulting from the combined effects of relativistic Doppler beaming and gravitational light bending ([Kamruddin & Dexter 2013](#)); in the second one, an edge-detection scheme and a pattern-matching algorithm are introduced to measure the properties of the black hole shadow even if the latter has an arbitrary shape ([Psaltis et al. 2014](#)). (ii) They assume that the observer knows the exact position of the centre of black hole<sup>4</sup>. (iii) They are restricted to a very specific measure of the distortion and are unable to model arbitrary distortion; exceptions are the works of [Johannsen & Psaltis \(2010\)](#) and [Johannsen \(2013\)](#), where instead polar-averaged distortions have been proposed.

To counter these potential difficulties, we present here a new general formalism that is constructed to avoid the limitations mentioned above. In particular, we assume that the shadow has an arbitrary shape and expand it in terms of Legendre polynomials in a coordinate system with origin in the effective centre of the shadow. This approach gives us the advantage of not requiring the knowledge of the centre of the black hole and of allowing us to introduce a number of parameters that measure the distortions of the shadow. These distortions are both accurate and robust, and can be implemented in a coordinate independent manner by different teams analysing the same noisy data.

The paper is organized as follows. In Sect. 2 we develop the new coordinate-independent formalism, where an arbitrary black hole shadow is expanded in terms of Legendre polynomials. Using this formalism, we introduce in Sect. 3 various distortion parameters of the shadow. In Sect. 4 we apply the formalism to a number of black hole space-times by computing the coefficients of the expansion and by showing that they exhibit an exponentially rapid convergence. We also compare the properties of the different distortion parameters and assess which definition appears to be more accurate and robust in general. Section 5 offers a comparison between the new distortion parameters introduced here with the more traditional ones simulating the noisy data that are expected from the observations. Finally, Sect. 6 summarizes our main results the prospects for the use of the new formalism.

We use a system of units in which  $c = G = 1$ , a space-like signature  $(-, +, +, +)$  and a spherical coordinate system  $(t, r, \theta, \phi)$ . Greek indices are taken to run from 0 to 3.

<sup>2</sup> <http://eventhorizontelescope.org/>

<sup>3</sup> <http://blackholecam.org/>

<sup>4</sup> The reconstruction procedures of the observational data does resolve this problem, which is however still present when considering and comparing purely theoretical representations of the shadow

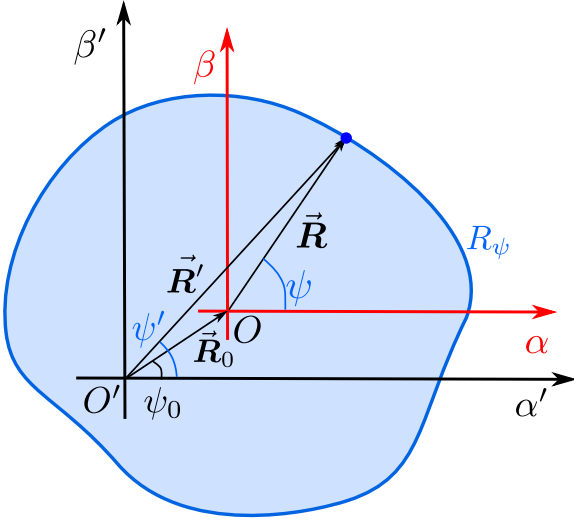


**Figure 1.** Schematic representation of the black hole shadow as a generic polar curve  $R_\psi$  in a coordinate system  $(\alpha, \beta)$  with origin  $O$  in the ‘centre’ of the shadow. The latter is translated by a vector  $\vec{R}_0$  with respect to the arbitrary coordinate system  $(\alpha', \beta')$  with origin  $O'$  in which the observations are made.

## 2 GENERAL CHARACTERIZATION OF THE SHADOW

In what follows we develop a rather general formalism to describe the black hole shadow that radio astronomical observations are expected to construct. For all practical purposes, however, we will consider the problem not to consist of the determination of the innermost unstable circular orbits for photons near a black hole. Rather, we will consider the problem of characterizing in a mathematically sound and coordinate-independent way a closed curve in a flat space, as the one in which the image will be available to us as distant observers.

Assume therefore that the astronomical observations provide the shadow as an one-dimensional closed curve defined by the equation

$$R' = R'(\psi'), \quad (1)$$

where  $R'$  and  $\psi'$  can be thought of as the radial and angular coordinates in a polar coordinate system with origin in  $O'$ . In practice, astronomical observations will not be able to provide such a sharp closed line and a more detailed analysis would need to take the observational uncertainties (which could well be a function of  $\psi'$ ) into account. We will discuss some of these uncertainties in Sect. 5, but for the time being we will consider the shadow as an idealized one-dimensional closed curve. A schematic example of the polar curve is shown in Fig. 1, where  $\alpha'$  and  $\beta'$  are the so-called ‘‘celestial coordinates’’ of the observer, and represent an orthogonal coordinate system with one of the unit vectors being along the line of sight.

Of course, there is no reason to believe that such a coordinate system is particularly useful, or that in using it a nonrotating black hole will have a shadow given by a perfect circle. Hence, in order to find a better coordinate system, and, in particular, one in which a Schwarzschild black hole has a circular shadow, we define the *effective centre* of the curve extending the definition of the position

of the centre of mass for a solid body to obtain

$$\vec{R}_0 := \frac{\int_0^{2\pi} \vec{e}_{R'}(\psi') R' [g_{R'R'}(dR'/d\psi')^2 + g_{\psi'\psi'}]^{1/2} d\psi'}{\int_0^{2\pi} [g_{R'R'}(dR'/d\psi')^2 + g_{\psi'\psi'}]^{1/2} d\psi'}, \quad (2)$$

where  $\vec{e}_{R'}$  is the radial-coordinate unit vector and where  $g_{R'R'}$ ,  $g_{\psi'\psi'}$  are the metric functions of the polar coordinate system  $(R', \psi')$ . Two important remarks: first, radio observations may well yield, especially in the nearest future, only a portion of the shadow, namely, the one with the largest brightness. Yet, it is useful to consider here the shadow as a closed polar curve since this is the way it is normally discussed in purely theoretical investigations. Second, at least observationally, the location of the centre of the black hole shadow is a free parameter in the image-reconstruction procedure and so already part of the analysis of the observational data. At the same time, the definition of a centre is useful also in the absence of actual observational data since it can help in the comparison of shadows that are built analytically and hence without observational data.

From the knowledge of the vector  $\vec{R}_0$ , the coordinate position of the effective centre can be expressed explicitly in terms of the radial and angular coordinates as

$$R_0 := \left( \int_0^{2\pi} R' d\psi' \right)^{-1} \left[ \left( \int_0^{2\pi} R'^2 \cos \psi' d\psi' \right)^2 + \left( \int_0^{2\pi} R'^2 \sin \psi' d\psi' \right)^2 \right]^{1/2}, \quad (3)$$

$$\psi_0 := \tan^{-1} \left( \frac{\int_0^{2\pi} R'^2 \sin \psi' d\psi'}{\int_0^{2\pi} R'^2 \cos \psi' d\psi'} \right). \quad (4)$$

We note that if the centre of the primary coordinate system  $O'$  coincides with the black hole origin, then the parameter  $R_0$  exactly corresponds to the shift of the centre of the shadow with respect to the black hole position defined by Tsukamoto et al. (2014).

Having determined the effective centre of the shadow, it is convenient to define a new polar coordinate system centred in it with coordinates  $(R, \psi)$ . Clearly, the new coordinate system with origin  $O$  is just translated by  $\vec{R}_0$  with respect to  $O'$  and, hence, the relation between the two coordinate systems is given by

$$R := \left[ (R' \cos \psi' - R_0 \cos \psi_0)^2 + (R' \sin \psi' - R_0 \sin \psi_0)^2 \right]^{1/2}, \quad (5)$$

$$\psi := \tan^{-1} \frac{R' \sin \psi' - R_0 \sin \psi_0}{R' \cos \psi' - R_0 \cos \psi_0}. \quad (6)$$

Note that we have kept the new axes  $\alpha$  and  $\beta$  parallel to the original ones  $\alpha'$  and  $\beta'$ . This is not strictly necessary but given the arbitrariness of the orientation of both sets of axes, it provides a useful simplification.

A well-defined centre of coordinates allows us now to obtain a robust definition of the reference *areal circle* as the circle having the same area as the one enclosed by the shadow. In particular, given the closed parametric curve  $R = R(\psi)$ , its area will in general be given by

$$\begin{aligned} \mathcal{A} &:= \int_{\psi_1}^{\psi_2} d\psi \int_0^R \sqrt{g_{RR} g_{\psi\psi}} dR \\ &= \frac{1}{2} \int_{\psi_1}^{\psi_2} R^2 d\psi = \frac{1}{2} \int_{\lambda_1}^{\lambda_2} R^2(\lambda) \left( \frac{d\psi}{d\lambda} \right) d\lambda, \end{aligned} \quad (7)$$

where in the second equality we have set  $g_{RR} = 1$ ,  $g_{\psi\psi} = R(\psi)$ ,

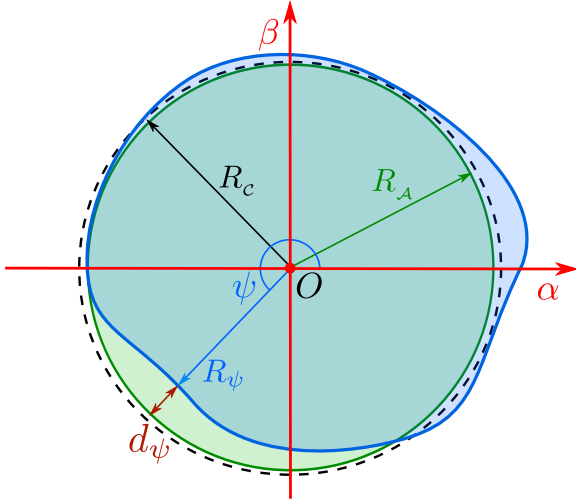


**Figure 2.** Schematic representation of the local distortion  $d_\psi$  between the polar curve  $R_\psi$  representing the black hole shadow and representative circles with circumference and area radii  $R_c$  and  $R_A$ , respectively.

while in the third equality we consider the representation of the curve in terms of a more generic parameter  $\lambda$ , i.e.,  $R = R(\psi(\lambda))$ . If the shadow is a closed curve, the integration limits  $\lambda_{1,2}$  can be found from the condition  $\psi(\lambda) = 0$  and  $\psi(\lambda) = 2\pi$ , while they will be restricted by the actual observational data when only a portion of the shadow is available.

We can then define the *areal radius*  $R_A$  of the reference circle simply as

$$R_A := \left(\frac{A}{\pi}\right)^{1/2}. \quad (8)$$

Similarly, and if simpler to compute, it is possible to define the *circumferential radius*  $R_c$  of the reference circle as

$$R_c := \frac{C}{2\pi}, \quad (9)$$

where the circumference is calculated as

$$\begin{aligned} C &:= \int (dR^2 + g_{\psi\psi} d\psi^2)^{1/2} \\ &= \int_{\lambda_1}^{\lambda_2} \left[ \left(\frac{dR}{d\lambda}\right)^2 + R^2 \left(\frac{d\psi}{d\lambda}\right)^2 \right]^{1/2} d\lambda. \end{aligned} \quad (10)$$

An areal radius is particularly useful as it enables one to measure two useful quantities, namely, the local deviation of the shadow  $R_\psi := R(\psi)$  from the areal circle, i.e.,

$$d_\psi := |R_A - R_\psi|, \quad (11)$$

and its polar average

$$d_{\langle\psi\rangle} := \frac{1}{2\pi} \int_0^{2\pi} d_\psi d\psi = \frac{1}{2\pi} \int_0^{2\pi} |R_A - R_\psi| d\psi. \quad (12)$$

Note that although similar, the areal and the circumferential radii are in general different and coincide just for a spherically symmetric black hole, in which case  $R_A = R_c = R_\psi$ , and of course  $d_\psi = 0 = d_s$ . All of these geometrical quantities are shown schematically in Fig. 2.

### 3 DISTORTION PARAMETERS

With a well defined and unambiguous set of coordinates  $(R, \psi)$ , we can next move to the characterization of the geometrical properties of the shadow. To this scope we simply employ an expansion in terms of Legendre polynomial, i.e., we define

$$R_\psi := \sum_{\ell=0}^{\infty} c_\ell P_\ell(\cos \psi), \quad (13)$$

where  $P_\ell(\cos \psi)$  is the Legendre polynomial of order  $\ell$  and the coefficients  $c_\ell$  of the expansion (13) can be found as

$$\begin{aligned} c_\ell &:= \frac{2\ell + 1}{2} \int_0^\pi R(\psi) P_\ell(\cos \psi) \sin \psi d\psi \\ &= \frac{2\ell + 1}{2} \int_{\lambda_1}^{\lambda_2} R(\psi) P_\ell(\cos \psi) \sin \psi \left(\frac{d\psi}{d\lambda}\right) d\lambda. \end{aligned} \quad (14)$$

The integration limits  $\lambda_{1,2}$  can be found from the condition  $\psi(\lambda) = 0$  and  $\psi(\lambda) = \pi$ , respectively. Using this decomposition, it is straightforward to measure the differences between the value of the parametrized shadow at two different angles. For example, the relative difference between the shadow at  $\psi = 0$  and at a generic angle  $\psi = \pi/m$  can be computed simply as

$$\begin{aligned} \delta_m &:= \frac{R_\psi(\psi = 0) - R_\psi(\psi = \pi/m)}{R_\psi(\psi = 0)} \\ &= 1 - \frac{\sum_{\ell=0}^{\infty} c_\ell P_\ell(\cos \psi)|_{\psi=\pi/m}}{\sum_{\ell=0}^{\infty} c_\ell P_\ell(\cos \psi)|_{\psi=0}}. \end{aligned} \quad (15)$$

When  $m = 1$ , expression (15) simplifies to

$$\delta_1 := 1 - \frac{\sum_{\ell=0}^{\infty} (-1)^\ell c_\ell}{\sum_{\ell=0}^{\infty} c_\ell}, \quad (16)$$

while, when  $m = 2$ , the difference can still be computed analytically and is given by

$$\delta_2 := 1 - \frac{\mathcal{B}}{\mathcal{A}}, \quad (17)$$

where we have introduced the following and more compact notation that will be used extensively in the remainder

$$\mathcal{A} := R_\psi(\psi = 0) = \sum_{\ell=0}^{\infty} c_\ell, \quad (18)$$

$$\mathcal{B} := R_\psi(\psi = \pi/2) = \sum_{\ell=0}^{\infty} (-1)^\ell \frac{(2\ell)!}{2^{2\ell} (\ell!)^2} c_{2\ell}, \quad (19)$$

$$\mathcal{C} := R_\psi(\psi = 3\pi/2) = \sum_{\ell=0}^{\infty} (-1)^\ell c_\ell. \quad (20)$$

Analytic expressions for (15) when  $m > 2$  are much harder to derive, but can be easily computed numerically.

We note that the parametrization (15) is quite general and allows us to recover in a single definition some of the expressions characterizing the distortion of the shadow and that have been introduced by other authors. For example, the parameter  $\delta_n^1$  can be associated to the distortion parameter  $\delta$  first introduced by [Hioki & Maeda \(2009\)](#) (cf. Fig. 3 of [Hioki & Maeda 2009](#)). Similarly, the parameter  $\delta_4$  is directly related to the distortion parameter  $\epsilon$  introduced by [Tsukamoto et al. \(2014\)](#) (cf. Fig. 3 of [Tsukamoto et al. 2014](#)).

In what follows we will exploit the general expression for the polar curve representing the black hole shadow to suggest three different definitions that measure in a coordinate-independent manner the amount of distortion of the shadow relative to some simple

background curve, e.g., a circle. These expressions are all mathematically equivalent and the use of one over the other will depend on the specific properties of the observed shadow.

### 3.1 Distortion parameter – I

We start by considering three points on the polar curve  $A$ ,  $B$ , and  $D$ , which occupy precise angular positions at  $\psi = 0$ ,  $\pi/2$ , and  $3\pi/2$ , respectively (see diagram in Fig. 3). The corresponding distances  $OA$ ,  $OB$  and  $OD$  from the centre of coordinates  $O$  can then be expressed as

$$R_A := R_\psi(\psi = 0) = \sum_{\ell=0}^{\infty} c_\ell P_\ell(\cos \psi)|_{\psi=0} = \mathcal{A}, \quad (21)$$

$$R_B := R_\psi(\psi = \pi/2) = \sum_{\ell=0}^{\infty} c_\ell P_\ell(\cos \psi)|_{\psi=\pi/2} = \mathcal{B}, \quad (22)$$

$$R_D := R_\psi(\psi = 3\pi/2) = R_B, \quad (23)$$

where in the last equality we have exploited the fact that the expansion in Legendre polynomials is symmetric with respect to the  $\alpha$  axis.

Next, we define a new parametric curve for which  $R_A = R_B = R_D$  and thus that satisfies the following condition

$$\mathcal{B} = \mathcal{A}, \quad (24)$$

or, equivalently, for  $\ell > 0$

$$c_{2\ell-1} = c_{2\ell} \left[ (-1)^\ell \frac{(2\ell)!}{2^{2\ell}(\ell!)^2} - 1 \right]. \quad (25)$$

The corresponding polar expression, formulated in terms of the Legendre polynomials expansion (13), is therefore given by

$$R_{\psi,I}(\psi) = c_0 + \sum_{\ell=1}^{\infty} c_{2\ell-1} \times \left\{ P_{2\ell-1}(\cos \psi) + \left[ (-1)^\ell \frac{(2\ell)!}{2^{2\ell}(\ell!)^2} - 1 \right]^{-1} P_{2\ell}(\cos \psi) \right\}, \quad (26)$$

To measure the distortion we need a reference curve, which we can choose to be the circle passing through the three points  $A$ ,  $B$ , and  $D$  and thus with radius

$$R_{s,I} := R_A = \mathcal{B} = R_B = \mathcal{A}. \quad (27)$$

We can now compute the deviation of the parametric curve (26) from the corresponding background circle of radius  $R_{s,I}$  at any angular position. However, as customary in this type of considerations, we can consider the shadow to be produced by a rotating black hole with spin axis along the  $\beta$  axis, so that the largest deviations will be on the axis of negative  $\alpha$  (this is shown schematically in the left-hand panel of Fig. A1, when considering the case of a Kerr black hole). More specifically, we can define the difference between the curves at  $\psi = \pi$  as

$$\begin{aligned} d_{s,I} &:= R_{s,I} - R_{\psi,I}(\psi = \pi) = \mathcal{B} - \sum_{\ell=0}^{\infty} c_{2\ell} + \sum_{\ell=1}^{\infty} c_{2\ell-1} \\ &= 2 \sum_{\ell=1}^{\infty} c_{2\ell-1}. \end{aligned} \quad (28)$$

It follows that our first definition for the dimensionless distortion

parameter –  $\delta_{s,I}$  can then be given by

$$\delta_{s,I} := \frac{d_{s,I}}{R_{s,I}} = \frac{2 \sum_{\ell=1}^{\infty} c_{2\ell-1}}{\mathcal{B}} =: \sum_{\ell=1}^{\infty} \delta_{\ell,I}, \quad (29)$$

which reduces to the compact expression

$$\delta_{s,I} \simeq \frac{2c_1}{c_0} = \delta_{1,I}. \quad (30)$$

when only the first two coefficients in the expansion are taken into account, i.e., for  $c_0 \neq 0 \neq c_1$  and  $c_\ell = 0$ , with  $\ell \geq 2$  (we recall that  $\delta_{0,I} = 0$ ). We also note that the assumption (27) does not restrict the analysis to spherically symmetric black hole space-times and, as we will show in Fig. 6, the distortion parameter (29) can be applied also to axisymmetric space-times.

### 3.2 Distortion parameter – II

A second possible definition of the distortion parameter is slightly more general and assumes that the radial distance of points  $A$  and  $B$  from the centre of coordinates is not necessarily the same, i.e.,  $R_A \neq R_B$ . In this case, one can think of introducing a new point  $E$  on the  $\alpha$  axis (this is shown schematically in the middle panel of Fig. A1, when considering the case of a Kerr black hole), such that the distances  $AE = EB$  and which could therefore serve as the centre of the reference circle. Since the values of the coordinates  $R_A$  and  $R_B$  are defined by expressions (21) and (22), we can use the condition  $AE = EB$  to find that one can easily find position of the point  $E$  on the  $\alpha$  axis is given by

$$R_E = \left| \frac{R_B^2 - R_A^2}{2R_A} \right|, \quad (31)$$

with the corresponding angular position  $\psi_E$  being either 0 or  $\pi$ , i.e.,

$$\psi_E = \cos^{-1} \left( \frac{R_A - R_B}{|R_A - R_B|} \right). \quad (32)$$

The radius of the circle passing through the three points  $A$ ,  $B$ , and  $D$  is

$$R_{s,II} = \frac{R_B^2 + R_A^2}{2R_A}, \quad (33)$$

so that the deviation of the shadow at  $\psi = \pi$  from the circle of radius  $R_{s,II}$  can be found using the relation

$$d_{s,II} = 2R_{s,II} - (R_A + R_C). \quad (34)$$

Finally, we can introduce the distortion parameter  $d_{s,II}$  defined as

$$d_{s,II} := \frac{\mathcal{B}^2}{\mathcal{A}} - \mathcal{C}, \quad (35)$$

so that the second dimensionless distortion parameter is expressed as

$$\delta_{s,II} := \frac{d_{s,II}}{R_{s,II}} = 2 \left( \frac{\mathcal{B}^2 - \mathcal{A}\mathcal{C}}{\mathcal{B}^2 + \mathcal{A}^2} \right). \quad (36)$$

The expression for the dimensionless distortion (36) is in this case more complex than the one presented in Eq. (29); however, in the simpler case in which only the lowest order coefficients are retained, i.e., if  $c_0 \neq 0 \neq c_1$  and  $c_\ell = 0$  for  $\ell \geq 2$ , we have

$$\delta_{s,II} \simeq \frac{2c_1^2}{2c_0^2 + 2c_0c_1 + c_1^2} = \delta_{1,II}. \quad (37)$$

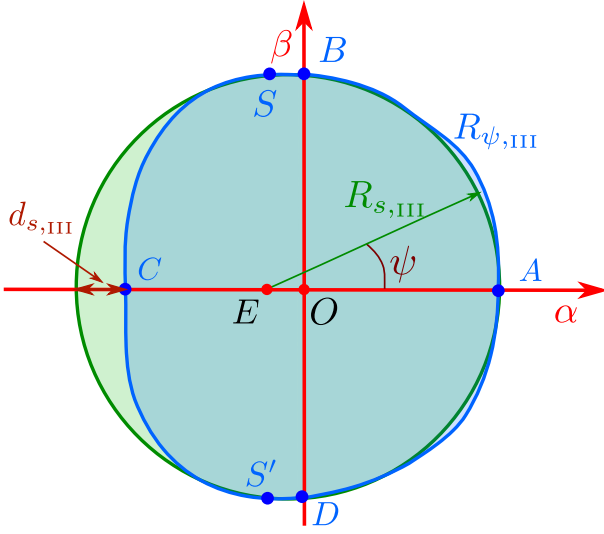


**Figure 3.** Schematic representation of the distortion parameter – III. The quantity  $d_{s,\text{III}}$  measures the difference between the Legendre expanded polar curve  $R_{\psi,\text{III}}$  and the reference circle of radius  $R_{s,\text{III}}$  and passing through the points  $A, B, D$ , and having centre in point  $E$ . Also shown are the “zero-slope” points  $S$  and  $S'$ .

### 3.3 Distortion parameter – III

A third and possibly *optimal* definition of the distortion parameter is one that is meant to consider the case in which the shadow is still reflection symmetric relative to the  $\alpha$  axis, but does not cross the  $\beta$  axis with a zero slope. Rather, the curve admits a point, say  $S$ , at angular position  $0 < \psi_S < \pi$ , where it has zero slope relative to the  $(\alpha, \beta)$  coordinate system (see diagram in Fig. 3 and the right-hand panel of Fig. A1 for the case of a Kerr black hole). This point will be referred to as the “slope point” of the parametric curve  $R_\psi$  representing the shadow.

To compute the position of this point in the  $(\alpha, \beta)$  coordinates we simply need to find the solution to the equation

$$\left. \frac{d\beta}{d\alpha} \right|_{\psi_S} = 0, \quad (38)$$

or, equivalently, solve for the differential equation

$$\frac{dR_\psi}{d\psi} \sin \psi + R_\psi \cos \psi = 0. \quad (39)$$

Using the expansion in terms of Legendre polynomials (13), we can rewrite equation (39) as

$$\sum_{\ell=0}^{\infty} c_\ell P_\ell(x) x - \sum_{\ell=0}^{\infty} c_\ell \frac{dP_\ell(x)}{dx} (1-x^2) = 0, \quad (40)$$

where we have set  $x := \cos \psi$ . The solutions of (40) provide the positions of all the possible slope points in the parametric curve, and the solution is unique in the case in which the shadow  $R(\psi)$  is convex. The corresponding coordinates of the point  $S$  are then

$$R_S = \sum_{\ell=0}^{\infty} c_\ell P_\ell(x_S), \quad (41)$$

$$\psi_A = \cos^{-1}(x_S). \quad (42)$$

As for the second distortion parameter in Sect. 3.3, we set  $E$  to be the centre of the circle passing through the points  $A, S$ , and

$S'$ , where  $S'$  the point is symmetric to the point  $S$  with respect to the  $\alpha$  axis. Using the condition  $AE = ED$ , we obtain the solution

$$R_D = \left| \frac{\mathcal{A}^2 - (\sum_{\ell=0}^{\infty} c_\ell P_\ell(x_S))^2}{2 \sum_{\ell=0}^{\infty} c_\ell (1 - P_\ell(x_S) x_S)} \right|, \quad (43)$$

$$\psi_D = \cos^{-1} \left( \frac{R_D}{|R_D|} \right). \quad (44)$$

Also for this third case, the radius of the circle  $R_{s,\text{III}}$  passing through the three points  $A, S$ , and  $S'$ , the distortion parameter  $d_{s,\text{III}}$ , and its dimensionless version  $\delta_{s,\text{III}}$ , have respectively the form

$$R_{s,\text{III}} = \frac{\mathcal{A}^2 - 2x_S \mathcal{A} (\sum_{\ell=0}^{\infty} c_\ell P_\ell(x_S)) + (\sum_{\ell=0}^{\infty} c_\ell P_\ell(x_S))^2}{2 \sum_{\ell=0}^{\infty} c_\ell (1 - P_\ell(x_S) x_S)}, \quad (45)$$

$$d_{s,\text{III}} = 2R_{s,\text{III}} - (R_A + R_C) = \left( \sum_{\ell=0}^{\infty} c_\ell P_\ell(x_S) \right) \times \frac{(\sum_{\ell=0}^{\infty} c_\ell P_\ell(x_S) - x_S \sum_{\ell=1}^{\infty} c_{2\ell-1} - \mathcal{A} \mathcal{C})}{\sum_{\ell=0}^{\infty} c_\ell (1 - P_\ell(x_S) x_S)}, \quad (46)$$

$$\delta_{s,\text{III}} = \frac{d_{s,\text{III}}}{R_{s,\text{III}}} = 2 \left( \sum_{\ell=0}^{\infty} c_\ell P_\ell(x_S) \right) \times \frac{(\sum_{\ell=0}^{\infty} c_\ell P_\ell(x_S) - x_S \sum_{\ell=1}^{\infty} c_{2\ell-1} - \mathcal{A} \mathcal{C})}{\mathcal{A}^2 - 2x_S \mathcal{A} \sum_{\ell=0}^{\infty} c_\ell P_\ell(x_S) + (\sum_{\ell=0}^{\infty} c_\ell P_\ell(x_S))^2}. \quad (47)$$

We note that this definition is similar to the one proposed by [Hioki & Maeda \(2009\)](#), who measure the dimensionless distortion of the shadow as

$$\delta_{s,\text{HM}} := \frac{d_{s,\text{HM}}}{R_{s,\text{HM}}}, \quad (48)$$

where

$$d_{s,\text{HM}} := R_\psi(\psi = \pi) - R_{s,\text{HM}}, \quad (49)$$

and with  $R_{s,\text{HM}}$  being the radius of the circle passing through the points  $A, S$ , and  $S'$ . The most important difference with respect to the definition of [Hioki & Maeda \(2009\)](#) is that we here express the parametric curve in terms of the general Legendre expansion (13), while [Hioki & Maeda \(2009\)](#) assume the knowledge of  $R_\psi$  at  $\psi = \pi$ .

Also in this case, expressions (45)–(47) are not easy to handle analytically. However, in the simplest case in which the expansion (13) has only two nonvanishing terms, such that  $c_0 \neq 0 \neq c_1$  and  $c_\ell = 0$  for  $\ell \geq 2$ , Eq. (40) takes the more compact form

$$2c_1 x^2 + c_0 x - c_1 = 0, \quad (50)$$

with solution

$$x_S = -\frac{c_0}{4c_1} \pm \sqrt{\frac{c_0^2}{16c_1^2} + \frac{1}{2}}, \quad (51)$$

and where the  $+$  or  $-$  signs refer to when  $c_1 > 0$  and  $c_1 < 0$ , respectively. The corresponding quantities  $R_{s,\text{III}}$ ,  $d_{s,\text{III}}$  and  $\delta_{s,\text{III}}$  have in this case the following form

$$R_{s,\text{III}} = \frac{2c_0^2 + c_1^2(1+x_S) + 2c_0c_1(1+x_S)}{2[c_0 + c_1(1+x_S)]}, \quad (52)$$

$$d_{s,\text{III}} = \frac{c_1^2(1+x_S)}{c_0 + c_1(1+x_S)}, \quad (53)$$

$$\delta_{s,\text{III}} = \frac{2c_1^2(1+x_S)}{2c_0^2 + c_1^2(1+x_S) + 2c_0c_1(1+x_S)} = \delta_{1,\text{III}}. \quad (54)$$

If the shadow is perfectly circular with radius  $c_0$ , then  $c_1 = 0$  and expressions (52)–(54) show that  $R_{s,\text{III}} = c_0$ ,  $d_{s,\text{III}} = 0 = \delta_{s,\text{III}}$ , as expected.

#### 4 APPLICATION OF THE FORMALISM TO BLACK HOLE SPACE-TIMES

Having constructed a general formalism that allows us to describe in a coordinate-independent manner the black hole shadow and to measure its deformation, we are now ready to apply such a formalism to the specific case of some well-known space-time metrics referring to axisymmetric black holes. In particular, we will obviously start with the application of the formalism to a rotating (Kerr) black hole (in Sect. 4.1), to move over to a Bardeen black hole and to a Kerr-Taub-NUT black hole in Sect. 4.2. We note that we do not consider these last two examples of black holes because they are particularly realistic, but simply because they offer analytic line elements on which our formalism can be applied.

##### 4.1 Kerr black hole

We start with the Kerr space-time, whose line element in Boyer-Lindquist coordinates reads

$$ds^2 = - \left( 1 - \frac{2Mr}{\Sigma} \right) dt^2 - \frac{4aMr \sin^2 \theta}{\Sigma} dt d\phi + \left( r^2 + a^2 + \frac{2a^2 Mr \sin^2 \theta}{\Sigma} \right) \sin^2 \theta d\phi^2 + \frac{\Sigma}{\Delta} dr^2 + \Sigma d\theta^2, \quad (55)$$

where

$$\Sigma := r^2 + a^2 \cos^2 \theta, \quad \Delta := r^2 - 2Mr + a^2, \quad (56)$$

with  $M$  being the mass of the black hole and  $a := J/M$  its specific angular momentum.

Since the shape of the shadow is ultimately determined by the innermost unstable orbits of photons, hereafter we will concentrate on their equations for photons. In such a space-time, the corresponding geodesic equations take the form

$$\Sigma \left( \frac{dt}{d\lambda} \right) = \frac{AE - 2aMrL_z}{\Delta}, \quad (57)$$

$$\Sigma^2 \left( \frac{dr}{d\lambda} \right)^2 = \mathcal{R}, \quad (58)$$

$$\Sigma^2 \left( \frac{d\theta}{d\lambda} \right)^2 = \Theta, \quad (59)$$

$$\Sigma \left( \frac{d\phi}{d\lambda} \right) = \frac{2aMrE}{\Delta} + \frac{(\Sigma - 2Mr)L_z}{\Delta \sin^2 \theta}, \quad (60)$$

where  $\lambda$  is an affine parameter,

$$\mathcal{R} := E^2 r^4 + (a^2 E^2 - L_z^2 - Q) r^2 + 2M [(aE - L_z)^2 + Q] r - a^2 Q, \quad (61)$$

$$\Theta := Q (a^2 E^2 - L_z^2 \csc^2 \theta) \cos^2 \theta, \quad (62)$$

$$A := (r^2 + a^2)^2 - a^2 \Delta \sin^2 \theta, \quad (63)$$

and  $E$  and  $L_z$  are the photon's energy and the angular momentum, respectively. The quantity  $Q$

$$Q = p_\theta^2 + \cos^2 \theta \left( \frac{L_z^2}{\sin^2 \theta} - a^2 E^2 \right) \quad (64)$$

is the so-called Carter constant and  $p_\theta := \Sigma d\theta/d\lambda$  is the canonical momentum conjugate to  $\theta$ .

Using these definitions, it is possible to determine the unstable orbits as those satisfying the conditions

$$\mathcal{R}(\bar{r}) = \frac{\partial \mathcal{R}(\bar{r})}{\partial r} = 0, \quad \text{and} \quad \frac{\partial^2 \mathcal{R}(\bar{r})}{\partial r^2} \geq 0, \quad (65)$$

where  $\bar{r}$  is the radial coordinate of the unstable orbit. Introducing now the new parameters  $\xi := L_z/E$  and  $\eta := Q/E^2$ , the celestial coordinates  $\alpha$  and  $\beta$  of the image plane of the distant observer are given by (Bardeen et al. 1972)

$$\alpha = \frac{\xi}{\sin i}, \quad \beta = \pm (\eta + a^2 \cos^2 i - \xi^2 \cot^2 i)^{1/2}, \quad (66)$$

where  $i$  is the inclination angle of the observer's plane, that is, the angle between the normal to the observer's plane and the black hole's axis of rotation. In the case of the Kerr space-time (55) and after using the conditions (65), one can easily find that the values of  $\xi$  and  $\eta$  relative to the circular orbit ( $c$ ) are (Young 1976; Chandrasekhar 1998)

$$\xi_c = \frac{M(\bar{r}^2 - a^2) - \bar{r}(\bar{r}^2 - 2M\bar{r} + a^2)}{a(\bar{r} - M)}, \quad (67)$$

$$\eta_c = \frac{\bar{r}^3 [4a^2 M - \bar{r}(\bar{r} - 3M)^2]}{a^2(\bar{r} - M)^2}, \quad (68)$$

Next, to investigate the shape of the black hole shadow we introduce the generic celestial polar coordinates  $(R', \psi')$  (cf. Sect. 2 and Fig. 1) defined as

$$R' = (\alpha^2 + \beta^2)^{1/2}, \quad (69)$$

$$\psi' = \tan^{-1} \left( \frac{\beta}{\alpha} \right). \quad (70)$$

Assuming for simplicity that the observer is in the equatorial plane, i.e., that  $i = \pi/2$ , then in terms of the  $(R', \psi')$  coordinates the shadow of black hole can be described as (hereafter we will set  $M = 1$ )

$$R' = \frac{(2r^4 + 2a^2 r - 6r^2 + a^2 + a^2 r^2)^{1/2}}{r - 1}, \quad (71)$$

$$\psi' = \tan^{-1} \left( \frac{\{r^3 [4a^2 - r(r-3)^2]\}^{1/2}}{r^2 - a^2 - r(r^2 - 2r + a^2)} \right). \quad (72)$$

Making use of the procedure described in Sect. 2, it is straightforward to determine the coordinates (3)–(4) of the effective centre of the shadow, and to perform the Legendre expansion (13). To the best of our knowledge, no analytic expression exists to cast the coordinates (71)–(72) as a polar curve  $R_\psi = R(\psi)$ . However, such a curve can be easily constructed numerically and from it the Legendre expansion (13) can be computed.

Figure 4 summarizes the results of our approach by reporting in the left-hand panel and in a logarithmic scale the normalized values of the expansion coefficients  $c_\ell$  as a function of the Legendre order  $\ell$ . Different curves refer to the different values considered for the dimensionless spin parameter  $a^* := J/M^2 = a/M$ , which ranges from  $a^* = 0.4$  (blue solid line) to  $a^* = 0.99$  (red solid line). Interestingly, the series converges very rapidly (essentially exponentially) and already with  $\ell = 4$ , the contribution of higher-order terms is of the order of  $10^{-2}$ , decreasing further to  $\sim 10^{-3}$  for  $\ell = 6$ . Furthermore, even when considering the more severe test of  $a^* = 0.99$ , the expansion coefficient with  $\ell = 6$  is only a factor 2-3 larger than the corresponding coefficient for a slowly rotating black hole. The right-hand panel of Fig. 4 shows a direct measure of the relative differences between the polar curve

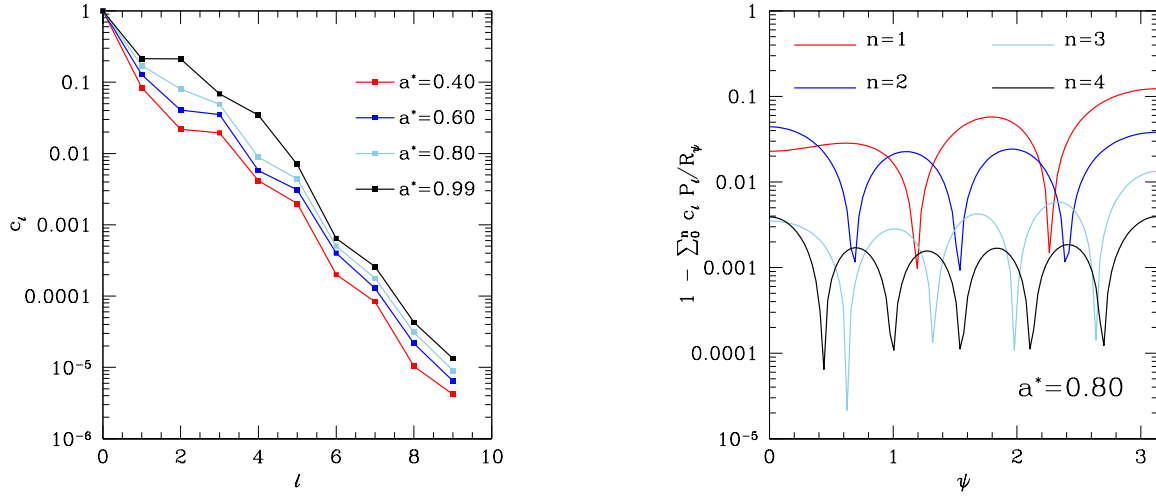


**Figure 4.** *Left-hand panel:* Magnitude of the expansion coefficients  $c_\ell$  of the polar curve and shown as a function of the expansion order. Note the very rapid (exponential) convergence of the expansion. The coefficients are computed for a Kerr black hole and different lines refer to different values of the spin parameter  $a^*$ . *Right-hand panel:* Relative differences between the polar curve for the black hole shadow as constructed from expressions (71)–(72) and the corresponding curve obtained from the expansion, i.e.,  $1 - \sum_0^n c_\ell P_\ell / R_\psi$ . Different lines refer to different truncations of the expansion and show that three coefficients are sufficient to obtain deviations of a few percent.

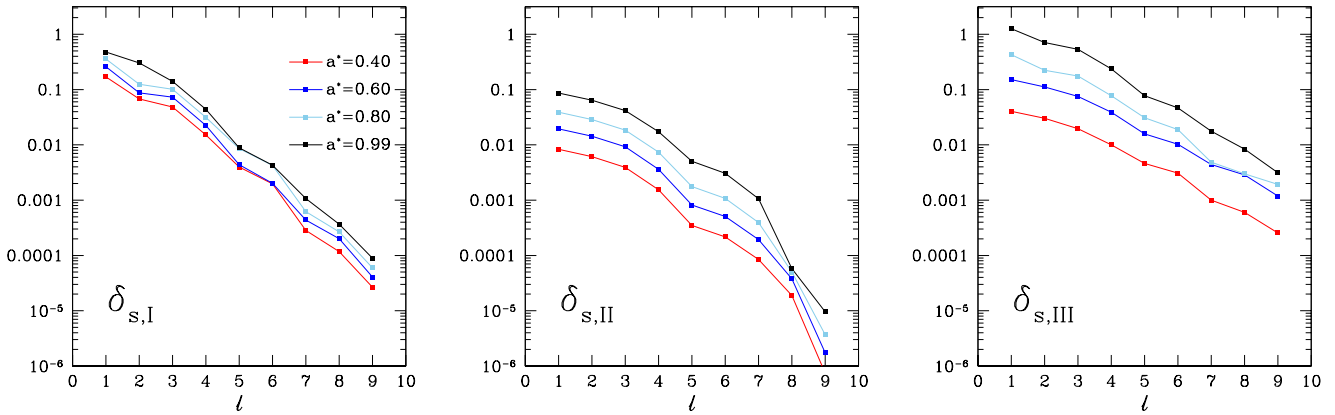


**Figure 5.** Magnitude as a function of the expansion order of the three different distortion parameters  $\delta_{s,I}$ – $\delta_{s,III}$  defined as in Eqs. (29), (36), and (47), thus measuring the difference between the Legendre expanded polar curves  $R_{\psi,I}$ – $R_{\psi,III}$  and the reference circles of radii  $R_{s,I}$ – $R_{s,III}$ . All curves refer to a Kerr black hole and different colours are used to represent different values of the spin parameter.

for the black hole shadow as constructed from expressions (71)–(72) and the corresponding curve obtained from the expansion, i.e.,  $1 - \sum_0^n c_\ell P_\ell / R_\psi$ . Remarkably, already when considering the first three terms in the expansion, i.e.,  $c_0$ ,  $c_1$ , and  $c_2$ , the relative difference is of a few percent (blue line), and this further reduces to  $10^{-3}$  when the expansion is truncated at  $n = 4$  (black line).

In summary, Fig. 4 demonstrates that when considering a Kerr black hole, the approach proposed here provides a coordinate independent and accurate representation of the black hole shadow and that a handful of coefficients is sufficient for most practical purposes. In the following Sections we will show that this is the case also for other axisymmetric black holes.

Before doing that, we show in Fig. 5 the values of the dimensionless distortion parameters as computed for the shadow of a Kerr black hole and for increasing values of the expansion index  $\ell$ . The three different panels are relative respectively to the parameters

(29), (36), and (47), with the different curves referring to values of the spin parameter  $a^*$ , ranging from  $a^* = 0.4$  (blue solid line) to  $a^* = 0.99$  (red solid line). As one would expect, for all values of  $a^*$ , each of the three distortion parameters decreases as the expansion includes higher-order terms. At the same time, because larger rotation rates introduce larger distortions in the shadow, they also lead to larger values of the distortion parameters for a fixed value of  $\ell$ .

Finally, Fig. 6 offers a comparative view of the different distortion parameters for specific values of the spin parameter, with the left-hand and right-hand panels referring to  $a^* = 0.4$  and  $a^* = 0.99$ , respectively. This view is rather instructive as it shows that the different definitions lead to significantly different values of the distortion, despite they all refer to the same parametric polar curve. Furthermore, it helps appreciate that the distortion parameter  $\delta_{s,II}$  is systematically smaller than the other two and hence not the

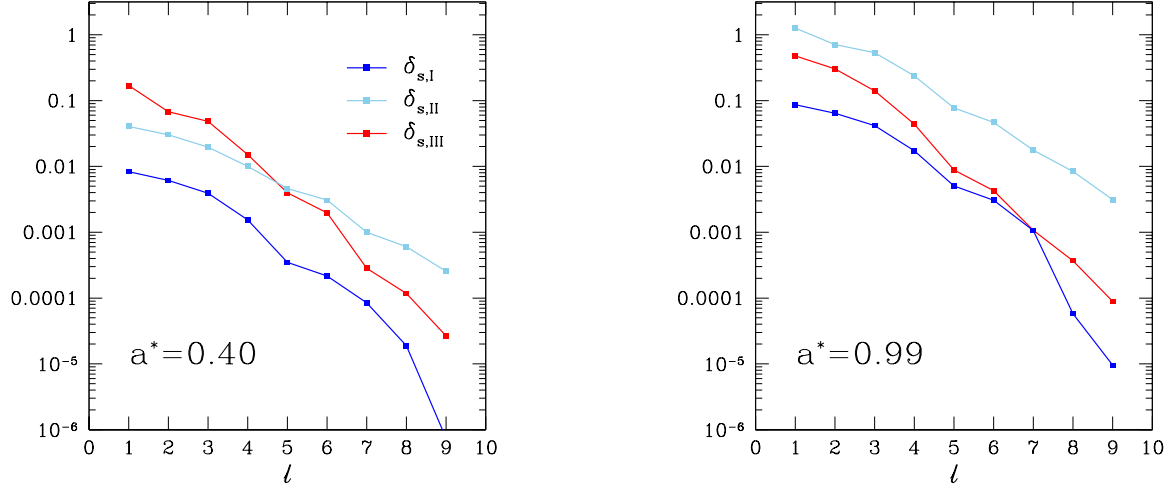


**Figure 6.** Comparative view of the different distortion parameters  $\delta_{s,I}$  (red line),  $\delta_{s,II}$  (blue line), and  $\delta_{s,III}$  (light-blue line). The left-hand and right-hand panels show the values of the distortion parameters as a function of the expansion order (cf. Fig. 5), and refer to a Kerr black hole with spin  $a^* = 0.40$  and  $a^* = 0.99$ , respectively.

optimal one. This is because a larger value of the distortion parameter will increase the possibility of capturing the complex structure of the shadow. The fact that the curves for  $\delta_{s,I}$  and  $\delta_{s,III}$  intersect for the Kerr black hole considered at  $\ell = 5$  implies that both distortion parameters (29) and (47) are useful indicators, with  $\delta_{s,III}$  being the recommended choice for expansions having  $\ell \geq 5$ .

#### 4.2 Bardeen and Kerr-Taub-NUT black holes

We continue our application of the formalism developed in Sects. 2 and 3 by considering the space-time of a rotating Bardeen black hole (Bardeen 1968). We recall that in Boyer-Lindquist coordinates, the metric of a Kerr and of a Bardeen black hole differ uniquely in the mass, which needs to be modified as (Bambi & Modesto 2013; Tsukamoto et al. 2014)

$$M \rightarrow m = M \left( \frac{r^2}{r^2 + g^2} \right)^{3/2}, \quad (73)$$

where the parameter  $g$  is the magnetic charge of the nonlinear electrodynamic field responsible for the deviation away from the Kerr space-time.

The impact parameters  $\xi$  and  $\eta$  relative to the circular orbit are in this case (Tsukamoto et al. 2014)

$$\xi_c = \frac{m[(2-f)\bar{r}^2 - fa^2] - \bar{r}(\bar{r}^2 - 2m\bar{r} + a^2)}{a(\bar{r} - fm)}, \quad (74)$$

$$\eta_c = \frac{\bar{r}^3 \{4(2-f)a^2m - \bar{r}[\bar{r} - (4-f)m]^2\}}{a^2(\bar{r} - fm)^2}, \quad (75)$$

and can be taken to define the shadow of black hole. Note that  $m$  and  $f$  are functions of the unstable circular radius  $\bar{r}$  and are given by

$$m = m(\bar{r}) = M \left( \frac{\bar{r}^2}{\bar{r}^2 + g^2} \right)^{3/2}, \quad (76)$$

$$f = f(\bar{r}) = \frac{\bar{r}^2 + 4g^2}{\bar{r}^2 + g^2}. \quad (77)$$

In complete analogy, we can consider a Kerr-Taub-NUT black

hole with nonvanishing gravitomagnetic charge  $n$  and specific angular momentum  $a := J/M$ . The corresponding metric is given by (Newman et al. 1963)

$$\begin{aligned} ds^2 = & -\frac{1}{\Sigma} (\Delta - a^2 \sin^2 \theta) dt^2 + \Sigma \left( \frac{dr^2}{\Delta} + d\theta^2 \right) \\ & + \frac{1}{\Sigma} [(\Sigma + a\chi)^2 \sin^2 \theta - \chi^2 \Delta] d\phi^2 \\ & + \frac{2}{\Sigma} (\Delta\chi - a(\Sigma + a\chi) \sin^2 \theta) dt d\phi, \end{aligned} \quad (78)$$

where the functions  $\Delta$ ,  $\Sigma$ , and  $\chi$  are now defined as

$$\begin{aligned} \Delta & := r^2 + a^2 - n^2 - 2Mr, \\ \Sigma & := r^2 + (n + a \cos \theta)^2, \\ \chi & := a \sin^2 \theta - 2n \cos \theta. \end{aligned} \quad (79)$$

In this case, the impact parameters  $\xi$  and  $\eta$  for the circular orbits are given by (Abdujabbarov et al. 2013)

$$\xi_c = \frac{a^2(1 + \bar{r}) + \bar{r}^2(\bar{r} - 3) + n^2(1 - 3\bar{r})}{a(1 - \bar{r})}, \quad (80)$$

$$\begin{aligned} \eta_c = \frac{1}{a^2(\bar{r} - 1)} \left\{ \bar{r}^3 [4a^2 - \bar{r}(\bar{r} - 3)^2] - n^2 [4\bar{r}^2 a^2 \right. \\ \left. + (1 - 3\bar{r})(n^2(1 - 3\bar{r}) - 6\bar{r}^2 + 4a^2\bar{r} + 2\bar{r}^3)] \right\}, \end{aligned} \quad (81)$$

and define the shadow of the Kerr-Taub-NUT black hole.

Applying the formalism described in Sect. 2, it is possible to compute the coefficients of the Legendre expansion (13) also for a Bardeen and for a Kerr-Taub-NUT black hole. The numerical values of these coefficients are reported as a function of the expansion order  $\ell$  in Fig. 7, where the left-hand panel refers to a Bardeen black hole, while the right-hand one to a Kerr-Taub-NUT black hole. More specifically, the different lines in the left-hand panel refer to different values of the magnetic charge:  $g = 0.00$  (red line),  $g = 0.30$  (blue line), and  $g = 0.60$  (light-blue line); all lines refer to a fixed value of the rotation parameter  $a^* = 0.60$ . Very similar is also the content of the right-hand panel of Fig. 7, which is however relative to a Kerr-Taub-NUT black hole. The different curves in this

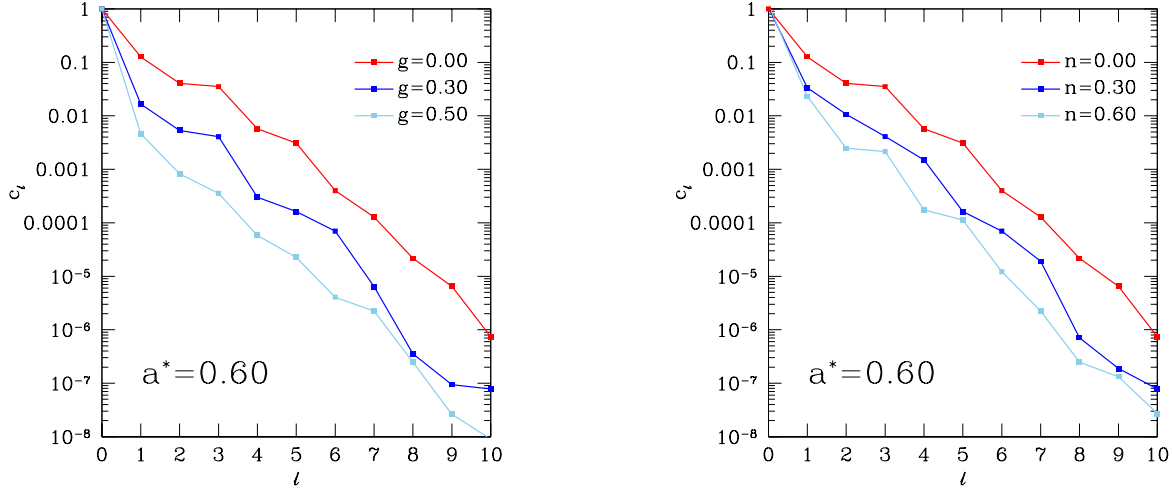


**Figure 7.** *Left-hand panel:* Magnitude of the expansion coefficients  $c_\ell$  as a function of the expansion order  $\ell$  for the different values of the magnetic charge of a Bardeen black hole:  $g = 0.00$  (red line),  $g = 0.30$  (blue line), and  $g = 0.50$  (light-blue line). All lines refer to a fixed value of the rotation parameter  $a^* = 0.60$  (cf. left panel of Fig. 4). *Right-hand panel:* The same as in the left-hand panel but for a Kerr-Taub-NUT black hole. Different curves refer to the different values of the NUT parameter:  $n = 0.00$  (red line),  $n = 0.30$  (blue line), and  $n = 0.60$  (light-blue line). All lines refer to a fixed value of the rotation parameter  $a^* = 0.60$ .

case refer to the different values of the NUT parameter:  $n = 0.00$  (red line),  $n = 0.30$  (blue line), and  $n = 0.60$  (light-blue line); once again, all lines refer to a fixed value of the rotation parameter  $a^* = 0.60$ .

In analogy with what shown in the left-hand panel of Fig. 4 for a Kerr black hole, also for these black holes the series converges very rapidly and already with  $\ell = 4$ , the contribution of higher-order terms is of the order of  $10^{-3}$ , decreasing further to  $\sim 10^{-5}$  for  $\ell = 6$ , even when considering higher larger magnetic charges or NUT parameters. Furthermore, in analogy with the right-hand panel of Fig. 4, we have checked that the relative differences between the polar curves for the shadow constructed from expressions (74)–(75) and (80)–(81), and the corresponding curve obtained from the expansion, i.e.,  $1 - \sum_0^n c_\ell P_\ell / R_\psi$ , is below  $10^{-2}$  when  $n = 2$  (not shown in Fig. 7); this difference further reduces to  $10^{-4}$  when the expansion is truncated at  $n = 4$ .

In conclusion, also Fig. 7 demonstrates that the approach proposed here provides a coordinate independent and accurate representation of black hole shadows in space-times other than the Kerr one.

## 5 COMPARISON WITH NOISY OBSERVATIONAL DATA

All of the considerations made so far have relied on the assumption that the shadow is a well-defined one-dimensional curve (cf. discussion in Sect 2). In practice, however, this is not going to be the case as the astronomical observations will have intrinsic uncertainties that, at least initially, will be rather large. It is therefore natural to ask how the formalism presented here will cope with such uncertainties. More precisely, it is natural to ask whether it will still be possible to determine the effective centre of a noisy polar curve and then determine from there its properties. Although a very obvious and realistic problem, this concern is systematically ignored in the literature, where the shadow is traditionally assumed to have no uncertainty due to the observational measurements.

While awaiting for actual observational data, we can straight-

forwardly address this issue in our formalism and mimic the noisiness in the observational data by considering the polar curve as given by the Legendre expansion (13), where however the different coefficients  $c_\ell$  are artificially perturbed. More specifically, we express the shadow via the new expansion

$$R_\psi = \sum_{\ell=0}^{\infty} c_\ell (1 + \Delta_c) P_\ell(\cos \psi), \quad (82)$$

where  $\Delta_c$  is a random real number chosen uniformly in the range  $[-\Delta_{\max}, \Delta_{\max}]$ . In this way, our putative polar curve representing the shadow will be distorted following a random distribution and we have optimistically assumed a variance of only 5%, i.e.,  $\Delta_{\max} = 0.05$ . Of course, there is no reason to expect that the error distribution in the actual observational data will be uniform, but assuming a white noise is for us the simplest and less arbitrary choice.

With the setup described above and the formalism discussed in the previous Sections, we have considered a reference shadow of a Kerr black hole with spin parameter  $a/M = 0.99$  and have reproduced it after truncating the expansion (82) at  $\ell = 9$ , which is more than sufficient given the accuracy obtained at this order (cf. Fig. 4). We have therefore constructed a very large number of such realizations of the observational shadow after making use of  $N_{\text{tot}} = 10^5$  draws of the random deformation  $\Delta_c$ . For each putative observed reconstructed shadow we have computed the distortion parameters  $\delta_{s,\text{I}} - \delta_{s,\text{III}}$  defined in Eqs. (29), (36), and (47), as well as the distortion definition of Hioki & Maeda (2009) and defined in Eq. (48).

For each of the shadow realizations we have therefore computed the measurement error as

$$\epsilon_* := \delta_s - \delta_{s,*}, \quad (83)$$

where  $\delta_s$  is the exact distortion of the background Kerr solution and measuring the relative difference of the shadow at  $\psi = 0$  and  $\psi = \pi$ . On the other hand,  $\delta_{s,*}$  is given by either  $\delta_{s,\text{I}} - \delta_{s,\text{III}}$  or  $\delta_{s,\text{HM}}$ .

Figure 8 shows the distributions of the errors computed in this

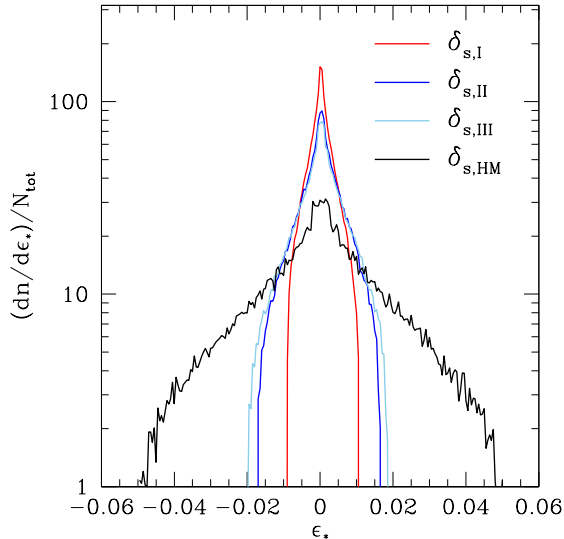


**Figure 8.** Comparison of probability density distributions of the errors  $\epsilon_*$  computed in the measurement of the distortion parameters  $\delta_{s,I} - \delta_{s,III}$  for a Kerr black hole shadow reconstructed using a perturbed expansion [cf. Eq. (82)]. Also shown is the distribution of the error measured when using the distortion parameter introduced by [Hioki & Maeda \(2009\)](#) and that has a larger variance.

way for the four different possible definitions of the distortion parameters, with the black line referring to the distortion parameter in Eq. (48), and the red, blue and light-blue lines referring to the definitions (29), (36), and (47), respectively. Note that the values of the probability densities distributions are reported in such a way that

$$\frac{1}{N_{\text{tot}}} \int_{-\infty}^{\infty} dn = \frac{1}{N_{\text{tot}}} \int_{-\infty}^{\infty} \left( \frac{dn}{d\epsilon_*} \right) d\epsilon_* = 1. \quad (84)$$

The distributions reported in Fig. 8 are rather self-explanatory. Clearly, all the different definitions are centred on  $\epsilon_* = 0$ , indicating that on average they provide a good measurement of the distortion. On the other hand, the variance of the different distribution is rather different. Overall, the distortion parameters  $\delta_{s,I} - \delta_{s,III}$  have comparable variances, with a slightly smaller variations for the definition  $\delta_{s,I}$ . However, the variance of the distortion parameter for  $\delta_{s,HM}$  is almost twice as large as the others and it essentially spans the 5% variation that we introduce in the random distortion  $\Delta_c$ . These results are rather reassuring as they indicate that new definitions are not only accurate, but also robust with respect to random white noise. Furthermore, they appear to be superior to other distortion measurements suggested in the past.

As a final remark we note that the introduction of the perturbations in the expansion (82) also has the effect of changing the position of the effective centre of the shadow and hence the values of  $\vec{R}_0$  and  $\psi_0$  [cf. Eqs. (2) and (4)]. Fortunately, such variations represent only a high-order error, which is much smaller than those measured by the distortion parameters, with maximum measured variance of the order of  $10^{-4}$ . As a result, the distortions reported in Fig. 8 are genuine measurements of the shadow and not artefacts introduced by the changes in the effective centres.

## 6 CONCLUSION

The radio-astronomical observations of the shadow of a black hole would provide convincing evidence about the existence of black holes. Further, the study of the shadow could be used to learn about extreme gravity near the event horizon and determine the correct theory of gravity in a regime that has not been explored directly so far. A number of different mathematical descriptions of the shadow have already been proposed, but all make use of a number of simplifying assumptions that are unlikely to be offered by the real observational data, e.g., the ability of knowing with precision the location of the centre of the shadow.

To remove these assumptions we have developed a new general and coordinate-independent formalism in which the shadow is described as an arbitrary polar curve expressed in terms of a Legendre expansion. Our formalism does not presume any knowledge of the properties of the shadow and offers a number of routes to characterize the properties of the curve. Because our definition of the shadow is straightforward and unambiguous, it can be implemented by different teams analysing the same noisy data.

The Legendre expansion used in our approach converges exponentially rapidly and we have verified that a number of coefficients less than ten is sufficient to reproduce the shadow with a precision of one part in  $10^5$ , both in the case of a Kerr black hole with spin parameter of  $a/M = 0.99$ , and in the case of Bardeen and Kerr-Taub-NUT black holes with large magnetic charges and NUT parameters. Furthermore, the use of a simple Legendre expansion has allowed us to introduce three different definitions of the distortion of the shadow relative to some reference circles. The comparison of the different definitions has allowed us to determine which of them is best suited to capture the complex structure of the shadow and its distortions.

Finally, again exploiting the advantages of the Legendre expansion, we were able to simulate rather simply the presence of observational random errors in the measurements of the shadow. Constructing a large number of synthetically perturbed shadows, we have compared the abilities of the different parameters to measure the distortion in the more realistic case of a noisy shadow. Overall, we have found that our new definitions have error distributions with comparable variances, but also that these are about a factor of 2 smaller than the corresponding variance measured when using more traditional definitions of the distortion. Given these results, the approach proposed here could be used in all those studies characterizing the shadows of black holes as well as in the analysis of the data from experimental efforts such as EHT and BHC.

## ACKNOWLEDGEMENTS

It is a pleasure to thank A. Grenzbach, Y. Mizuno, Z. Younsi, and A. Zhidenko for useful discussions and comments. We are also grateful to the referee, D. Psaltis, for comments and suggestions that have improved the presentation. This research was partially supported by the Volkswagen Stiftung (Grant 86 866) and by the ERC Synergy Grant “BlackHoleCam – Imaging the Event Horizon of Black Holes” (Grant 610058). AAA and BJA are also supported in part by the project F2-FA-F113 of the UzAS and by the ICTP through the projects OEA-NET-76, OEA-PRJ-29. AAA and BJA thank the Institut für Theoretische Physik, Goethe Universität for warm hospitality during their stay in Frankfurt.

## REFERENCES

- Abdujabbarov A., Atamurotov F., Kucukakca Y., Ahmedov B., Camci U., 2013, *Astrophys. Space Sci.*, 344, 429
- Amarilla L., Eiroa E. F., 2012, *Phys. Rev. D*, 85, 064019
- Amarilla L., Eiroa E. F., 2013, *Phys. Rev. D*, 87, 044057
- Amarilla L., Eiroa E. F., Giribet G., 2010, *Phys. Rev. D*, 81, 124045
- Atamurotov F., Abdujabbarov A., Ahmedov B., 2013a, *Astrophys. Space Sci.*, 348, 179
- Atamurotov F., Abdujabbarov A., Ahmedov B., 2013b, *Phys. Rev. D*, 88, 064004
- Baiotti L., Rezzolla L., 2006, *Phys. Rev. Lett.*, 97, 141101
- Bambi C., Freese K., 2009, *Physical Review D*, 79, 043002
- Bambi C., Modesto L., 2013, *Physics Letters B*, 721, 329
- Bambi C., Yoshida N., 2010, *Classical and Quantum Gravity*, 27, 205006
- Bardeen J., 1968, in *Proceedings of GR5* p. 174
- Bardeen J. M., 1973, in , *Black Holes*. Gordon and Breach, New York
- Bardeen J. M., Press W. H., Teukolsky S. A., 1972, *Astrophys. J.*, 178, 347
- Berti E., Cardoso V., Starinets A. O., 2009, *Class. Quantum Grav.*, 26, 163001
- Broderick A. E., Narayan R., 2007, *Class. Quantum Grav.*, 24, 659
- Chan C.-K., Psaltis D., Özel F., Narayan R., Sałowski A., 2015, *Astrophysical Journal*, 799, 1
- Chandrasekhar S., 1998, *The mathematical theory of black holes*. Oxford University Press., New York
- Chirenti C. B. M. H., Rezzolla L., 2007, *Class. Quantum Grav.*, 24, 4191
- Doeleman S. S., Fish V. L., Broderick A. E., Loeb A., Rogers A. E. E., 2009, *Astrophys. J.*, 695, 59
- Eiroa E. F., Sendra C. M., 2014, *European Physical Journal C*, 74, 3171
- Falcke H., Markoff S. B., 2013, *Class. Quantum Grav*, 30, 244003
- Falcke H., Melia F., Agol E., 2000, *Astrophys. J. Lett.*, 528, L13
- Gebhardt K., Adams J., Richstone D., Lauer T. R., Faber S. M., Gültekin K., Murphy J., Tremaine S., 2011, *Astrophysical Journal*, 729, 119
- Genzel R., Eisenhauer F., Gillessen S., 2010, *Reviews of Modern Physics*, 82, 3121
- Ghez A. M., Salim S., Weinberg N. N., Lu J. R., Do T., Dunn J. K., Matthews K., Morris M. R., Yelda S., Becklin E. E., Kremenek T., Milosavljevic M., Naiman J., 2008, *Astrophys. J.*, 689, 1044
- Grenzebach A., Perlick V., Lämmerzahl C., 2014, *Phys. Rev. D*, 89, 124004
- Grenzebach A., Perlick V., Lämmerzahl C., 2015, arXiv:1503.03036
- Hioki K., Maeda K.-I., 2009, *Phys. Rev. D*, 80, 024042
- Johannsen T., 2013, *Astrophys. J.*, 777, 170
- Johannsen T., Psaltis D., 2010, *Astrophys. J.*, 718, 446
- Kamruddin A. B., Dexter J., 2013, *Mon. Not. R. Astron. Soc.*, 434, 765
- Mazur P. O., Mottola E., 2004, *Proceedings of the National Academy of Science*, 101, 9545
- Newman E., Tamburino L., Unti T., 1963, *Journal of Mathematical Physics*, 4, 915
- Perlick V., 2004, *Living Reviews in Relativity*, 9
- Psaltis D., Narayan R., Fish V. L., Broderick A. E., Loeb A., Doeleman S. S., 2015, *Astrophysical Journal*, 798, 15
- Psaltis D., Özel F., Chan C.-K., Marrone D. P., 2014, ArXiv e-prints
- Rezzolla L., Zhidenko A., 2014, *Phys. Rev. D*, 90, 084009
- Schee J., Stuchlík Z., 2009, *International Journal of Modern Physics D*, 18, 983
- Takahashi R., 2004, *Astrophysical Journal*, 611, 996
- Tsukamoto N., Li Z., Bambi C., 2014, *Journal of Cosmology and Astroparticles*, 6, 43
- Young P. J., 1976, *Phys. Rev. D*, 14, 3281
- Zakharov A. F., 2014, *Phys. Rev. D*, 90, 062007

## APPENDIX A: GRAPHICAL REPRESENTATION OF DISTORTION PARAMETERS: KERR BLACK HOLES

To help in the visualization of the different distortion parameters introduced in Section 3, we here present their graphical representation when they are applied to the shadow of a Kerr black hole shadow with spin parameter  $a^* = 0.98$ . The left-hand panel of Fig. A1 represents the distortion parameter I in Sect. 3, where the reference circle is defined in a such a way that the points  $B, D$  and the centre of the reference circle are all on the vertical axis  $\beta$ . Hence, the difference of the radial coordinates of the point  $C$  of the shadow boundary and of the left-hand point of the circle intersecting the axis  $\alpha$  corresponds to the distortion parameter  $d_{s,I}$ .

Similarly, the middle panel of Fig. A1 refers to the distortion parameter II, where the reference circle passes through the points  $A$  and  $B$ , which are on the axis  $\beta$ . The centre of the reference circle is on the point  $E$  and does not coincide with the centre of the coordinate system. The position of the reference circle centre  $E$  is instead defined by Eq. (31). The difference of the radial coordinates of the point  $C$  of the shadow and of the left-hand point of the circle intersecting with the axis  $\alpha$  corresponds to the distortion parameter  $d_{s,II}$ .

Finally, the right-hand panel of Fig. A1 corresponds to the distortion parameter III, where the reference circle passes through the slope points  $S, S'$ , and the right-hand point  $A$  of the shadow intersecting the axis  $\alpha$ . The positions of the slope points are defined by solving Eq. (39). The centre of the reference circle does not coincide with the origin of the coordinate system and its position is defined by Eq. (43). The difference of the radial coordinates of the point  $C$  of the shadow and of the left-hand point of the circle intersecting the axis  $\alpha$  corresponds to the distortion parameter  $d_{s,III}$ .

Note that the radius of the reference circle radius depends on the definition used for the distortion parameter; hence the distortion parameters are also different for each definition.

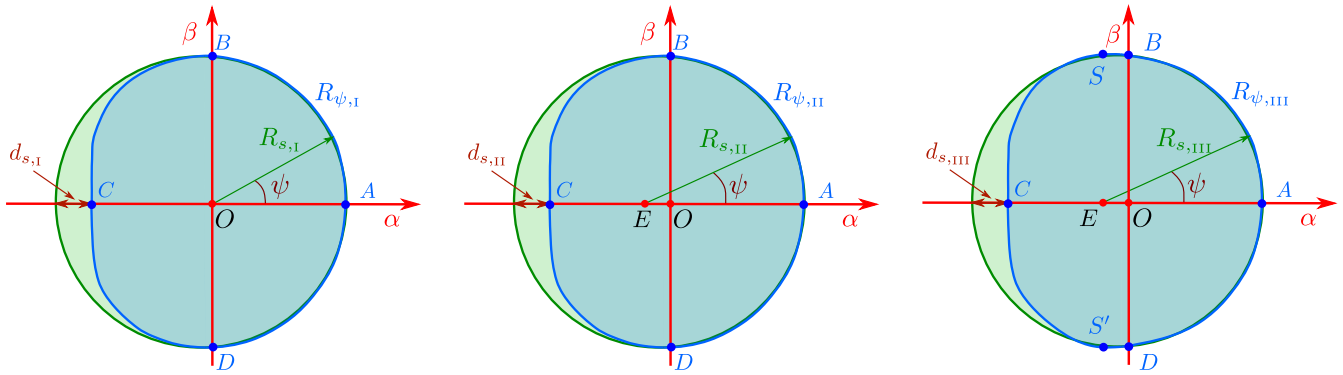


**Figure A1.** Schematic representations of the distortion parameters I, II and III when applied to the shadow of a Kerr black hole. The left-hand panel refers to the definition I, where the centre of the reference circle as well as the points  $B$  and  $D$  (which are not slope points) are on the coordinate axis  $\beta$ . The middle panel refers instead to definition II and in this case the centre of the reference circle  $E$  is displaced along the  $\alpha$  axis. Finally, the right-hand panel shows the representation of the definition III, where we consider the reference circle passing through the point  $A$  and the slope points  $B$  and  $D$  are not on the  $\beta$  axis. The centre of the reference circle  $E$  is also displaced and not exactly at the centre of the coordinate system.